




Band geometry induced high angular momentum excitonic superfluid in gapped chiral fermion systems

Huaiyuan Yang ¹, Yuelin Shao ^{2,3,*}, Yuanfeng Xu,⁴ Xi Dai,^{5,†} and Xin-Zheng Li ^{1,6,7,‡}

¹State Key Laboratory for Artificial Microstructure and Mesoscopic Physics, Frontier Science Center for Nano-optoelectronics and School of Physics, Peking University, Beijing 100871, People's Republic of China

²Beijing National Laboratory for Condensed Matter Physics and Institute of Physics, Chinese Academy of Sciences, Beijing 100190, People's Republic of China

³School of Physical Sciences, University of Chinese Academy of Sciences, Beijing 100049, People's Republic of China

⁴Center for Correlated Matter, School of Physics, Zhejiang University, No. 866, Yuhangtang Road, Xihu District, Hangzhou 310058, Zhejiang Province, People's Republic of China

⁵Department of Physics, Hong Kong University of Science and Technology, Clear Water Bay, Kowloon 999077, Hong Kong

⁶Interdisciplinary Institute of Light-Element Quantum Materials, Research Center for Light-Element Advanced Materials, and Collaborative Innovation Center of Quantum Matter, Peking University, Beijing 100871, People's Republic of China

⁷Peking University Yangtze Delta Institute of Optoelectronics, Nantong, Jiangsu 226010, People's Republic of China



(Received 20 January 2024; revised 26 March 2024; accepted 11 April 2024; published 3 May 2024)

We study the exciton condensation in the heterostructures where the electron layer and the hole layer formed by gapped chiral fermion (GCF) systems are separately gated. High angular momentum such as p - and d -wave-like excitonic pairing may emerge when the gap of the GCF systems is small compared to the Fermi energy, and the chiral winding numbers of the electrons and holes are the same. This is a result of the nontrivial band geometry and can be linked to the Berry curvature when projected onto the Fermi surface. In realistic systems, we propose that staggered graphene and surface states of magnetically doped topological insulators or intrinsic axion insulators are promising candidates for realizing p -wave exciton superfluid, and anomalous Hall conductivity can be used as a signature in experiments.

DOI: [10.1103/PhysRevB.109.L201401](https://doi.org/10.1103/PhysRevB.109.L201401)

Introduction. Composed of a bound electron-hole pair, an exciton is a charge-neutral Bosonic quasiparticle. In some specific systems such as intrinsic excitonic insulators or heterostructures formed by separated electron-hole layers, excitons can undergo Bose-Einstein condensation (BEC) and turn into superfluid [1–4]. Numerous theoretical works have predicted many nontrivial phenomena in p -wave exciton superfluid, including topologically protected vortex zero modes, charge fractionalization, parity anomaly, and non-Abelian braiding [5–8]. Up to now, the quantum well systems that have experimentally realized exciton condensation at very low temperature are based on graphene bilayers [9,10], as well as transition metal dichalcogenides (TMD) monolayers and moiré lattices [11–13], where the insulating block layers are hexagonal boron nitride and are several nanometers thick. However, all these exciton condensations are s -wave-like, regardless of whether in the BEC regime or the BCS regime, and the exciton superfluid has not been achieved in experiments yet. This has strongly hindered the progress in the field of this novel physics. Many proposals have been made in recent years to achieve p -wave excitonic pairing. Some discussed tunneling-assisted p -wave excitonic insulator

[14–16], but it is not a superfluid state as the phase transition there only corresponds to the breaking of discrete symmetries [17]. Peretto and Stefanucci found that Floquet engineering can help to realize nonequilibrium p -wave excitonic insulators [18]. However, an achievable system for equilibrium p -wave exciton superfluid is still absent.

One feature these previous works have in common is that the band geometry effects on exciton condensation have been neglected, and the band edges are described by the effective mass model. In the recent decade, however, many works have shown that this approximation breaks down when considering the exciton energy spectrum [19,20] and optical selection rules [21,22]. One can expect that the band geometry may also influence exciton condensation. This is especially true in gapped chiral fermion (GCF) systems, where the band geometry matters in many physical properties [19–28]. Many two-dimensional (2D) materials can be described by GCFs, e.g., gapped graphene monolayer and multilayers [29], gapped topological surface states [30], and many TMD monolayers like MoS₂ [25]. Therefore, a detailed exploration of the exciton condensation in GCF systems with band geometry taken into account is highly desired.

In this Letter, we study the band geometry effects on exciton condensation in charge-neutral hybrid heterostructures. The BCS regime is considered, where the separated electron and hole layers consisting of GCFs have definite Fermi surfaces (FSs). Through the analysis of the gap equation and

*ylshao@iphy.ac.cn

†daix@ust.hk

‡xzli@pku.edu.cn

numerical calculations, we find that high angular momentum such as p -wave and d -wave-like exciton condensation may appear when the chiral winding number of the electron and hole GCF systems are both 1 or both 2, and the gap of the GCFs is small compared to the gating voltage. Further, under the FS projection approximation, the angular momentum of the exciton condensation is found directly related to the Berry curvature flux enclosed in the electron and hole FSs. By increasing the total Berry curvature flux enclosed in the FSs, for example, increasing the charge density per layer, the exciton condensation might experience an s - to p -wave transition which will induce an integer jump of the anomalous Hall conductivity. For the material realization of the p -wave exciton condensation, we propose that staggered graphene and surface states of magnetically doped topological insulators or intrinsic axion insulators are promising candidates.

Model. We first introduce the 2D isotropic GCF model Hamiltonian for a single valley [22]:

$$H_{\text{GCF}} = \begin{pmatrix} D & \alpha k^{|w|} e^{iw\theta_k} \\ \alpha k^{|w|} e^{-iw\theta_k} & -D \end{pmatrix}, \quad (1)$$

where θ_k is the polar angle of \mathbf{k} . H_{GCF} describes the low-energy physics around a high-symmetry point of the system. The difference in the angular momentum between the conduction and valence bands is w , and the gap $2D > 0$ is approximately k -independent near the origin. $|w| = 1$ and $|w| = 2$ are the most common cases. TMDs and gapped graphene correspond to $|w| = 1$, while gated bilayer graphene [29] and topological excitonic insulator AsO and Mxene monolayers [31–33] correspond to $|w| = 2$. The eigenenergies are $\varepsilon_{c/v} = \pm \varepsilon_k = \pm \sqrt{D^2 + \alpha^2 k^{2|w|}}$, with eigenstates

$$|c\mathbf{k}\rangle = \begin{pmatrix} \cos \frac{\phi_k}{2} \\ \sin \frac{\phi_k}{2} e^{-iw\theta_k} \end{pmatrix}, \quad |v\mathbf{k}\rangle = \begin{pmatrix} \sin \frac{\phi_k}{2} e^{iw\theta_k} \\ -\cos \frac{\phi_k}{2} \end{pmatrix}, \quad (2)$$

where $\phi_k = \arccos(D/\varepsilon_k)$ and $\phi_k \in (0, \pi/2)$. Using this gauge, the lowest energy exciton state is a $1s$ state in the 2D hydrogen model [20,22]. Incorrect conclusions may be drawn if the gauge is not reasonably chosen [34].

The double-layer exciton condensation heterostructure is demonstrated in Fig. 1(a). Each layer is described by a GCF model. The top (bottom) layer is separately gated by V_t (V_b) so that the top (bottom) layer has an electron (hole) FS. In this Letter, we assume the charge neutral case ($V_{g,t} = -V_{g,b} = -V_g$), where the electron and hole FSs are perfectly nested as shown in Fig. 1(b), favoring the excitonic instability the most. After taking the electron-hole interaction into consideration, the formation of interlayer exciton condensation will open a gap [Fig. 1(c)], and the system evolves from a semimetal to an excitonic insulator.

The noninteracting Hamiltonian for the two-layer system in the two-band basis reads as follows:

$$H_0 = \sum_{\mathbf{k}} \Psi_{\mathbf{k}}^\dagger \begin{pmatrix} V_{g,t} + \varepsilon_{c\mathbf{k},t} & 0 \\ 0 & V_{g,b} + \varepsilon_{v\mathbf{k},b} \end{pmatrix} \Psi_{\mathbf{k}}, \quad (3)$$

where $\Psi_{\mathbf{k}}^\dagger = [c_{c\mathbf{k},t}^\dagger, c_{v\mathbf{k},b}^\dagger]$. Here $c_{c\mathbf{k},t}$ ($c_{v\mathbf{k},b}$) refers to the electrons in the conduction (valence) band of the top (bottom) layer in Fig. 1(b). The interlayer interaction between these two

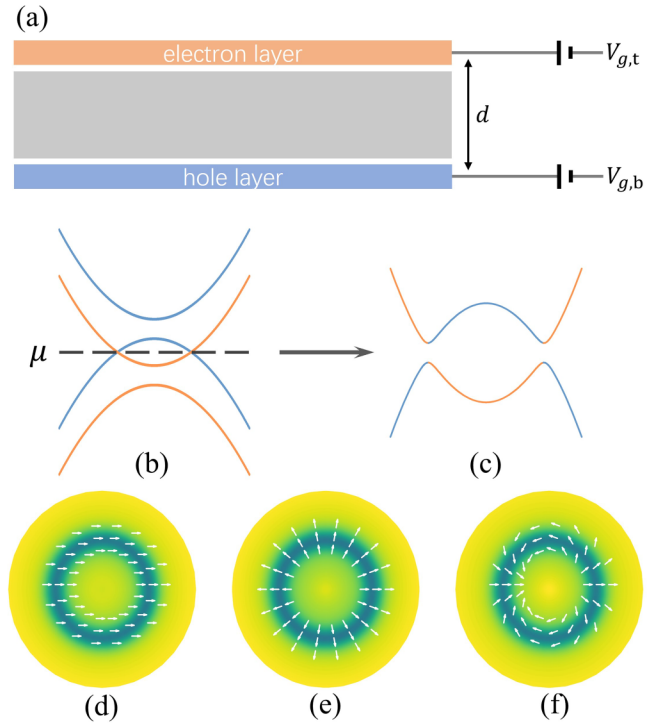


FIG. 1. (a) Schematic for the exciton condensation heterostructure. The electron and hole layers are separated in the z direction with a width d . (b) At the charge neutrality point, the electron and hole FSs are perfectly nested. (c) The excitonic instability is favored, and a gap opens. Here the orange (blue) lines indicate the bands from the top (bottom) layer. (d), (e), (f) s -, p -, d -wave-like excitonic order parameters. The direction of the arrow denotes the phase angle, and the darkness of the colormap indicates the magnitude.

bands reads as follows:

$$H_{\text{int}} = \frac{1}{S} \sum_{\mathbf{k}_1, \mathbf{k}_2, \mathbf{q}} V_{\text{inter}}(q) \Lambda_{cc}(\mathbf{k}_1, \mathbf{k}_1 - \mathbf{q}) \Lambda_{vv}(\mathbf{k}_2, \mathbf{k}_2 + \mathbf{q}) \times c_{c\mathbf{k}_1, t}^\dagger c_{v\mathbf{k}_2, b}^\dagger c_{v\mathbf{k}_2 + \mathbf{q}, b} c_{c\mathbf{k}_1 - \mathbf{q}, t}, \quad (4)$$

where $V_{\text{inter}}(q)$ is the interlayer screened Coulomb interaction, and $\Lambda_{ab}(\mathbf{k}, \mathbf{p}) \equiv \langle a\mathbf{k} | b\mathbf{p} \rangle$ is the form factor where $a, b \in \{c, v\}$. In GCF model, it deviates from unity:

$$\begin{aligned} \Lambda_{cc}(\mathbf{k}, \mathbf{p}) &= \cos\left(\frac{\phi_{c\mathbf{k}}}{2}\right) \cos\left(\frac{\phi_{c\mathbf{p}}}{2}\right) \\ &\quad + \sin\left(\frac{\phi_{c\mathbf{k}}}{2}\right) \sin\left(\frac{\phi_{c\mathbf{p}}}{2}\right) e^{im(\theta_{\mathbf{k}} - \theta_{\mathbf{p}})}, \\ \Lambda_{vv}(\mathbf{k}, \mathbf{p}) &= \cos\left(\frac{\phi_{v\mathbf{k}}}{2}\right) \cos\left(\frac{\phi_{v\mathbf{p}}}{2}\right) \\ &\quad + \sin\left(\frac{\phi_{v\mathbf{k}}}{2}\right) \sin\left(\frac{\phi_{v\mathbf{p}}}{2}\right) e^{-in(\theta_{\mathbf{k}} - \theta_{\mathbf{p}})}, \end{aligned} \quad (5)$$

where m (n) is the chiral winding number for the conduction (valence) band. Later we see that this band geometry effect plays an essential role in the excitonic pairing.

Gap equation. Using the standard Hartree-Fock approximation, we obtain the gap equation for the interlayer excitonic

pairing at 0 K:

$$\Delta_{\mathbf{k}} = \sum_{\mathbf{p}} V_{\text{inter}}(|\mathbf{k} - \mathbf{p}|) \Lambda_{cc}(\mathbf{k}, \mathbf{p}) \Lambda_{vv}(\mathbf{p}, \mathbf{k}) \frac{\Delta_{\mathbf{p}}}{2E_p S}, \quad (6)$$

where $2E_p$ is the quasiparticle excitation energy and S is the system area. For brevity, we only focus on the interlayer interaction, which is the primary factor, in the main text, and we present the details of the full Hartree-Fock equations in the Supplemental Material (SM) [35]. To analyze the excitonic pairing characteristics, we decompose the gap function into different angular momentum channels: $\Delta_{\mathbf{k}} = \sum_J |\Delta_{\mathbf{k}}|_J e^{iJ\theta_{\mathbf{k}}}$,

$J = 0, \pm 1, \pm 2, \dots$, and $|\Delta_{\mathbf{k}}|_J$ is independent of the polar angle [34]. In this way, Eq. (6) can be rewritten as independent equations for different J 's:

$$|\Delta_{\mathbf{k}}|_J = \sum_{\mathbf{p}} e^{-iJ(\theta_{\mathbf{k}} - \theta_{\mathbf{p}})} V_{\text{inter}}(|\mathbf{k} - \mathbf{p}|) \times \Lambda_{cc}(\mathbf{k}, \mathbf{p}) \Lambda_{vv}(\mathbf{p}, \mathbf{k}) \frac{|\Delta_{\mathbf{p}}|_J}{2E_p S}. \quad (7)$$

After inserting Eq. (5) into Eq. (7), and seeing that the imaginary parts of the exponentials are odd and vanish after the angle integration, we get

$$\begin{aligned} |\Delta_{\mathbf{k}}|_J = \sum_{\mathbf{p}} V_{\text{inter}}(|\mathbf{k} - \mathbf{p}|) \frac{|\Delta_{\mathbf{p}}|_J}{2E_p S} f_p \left[\cos\left(\frac{\phi_{ck}}{2}\right) \cos\left(\frac{\phi_{cp}}{2}\right) \cos\left(\frac{\phi_{vk}}{2}\right) \cos\left(\frac{\phi_{vp}}{2}\right) \cos J(\theta_{\mathbf{k}} - \theta_{\mathbf{p}}) \right. \\ + \cos\left(\frac{\phi_{ck}}{2}\right) \cos\left(\frac{\phi_{cp}}{2}\right) \sin\left(\frac{\phi_{vk}}{2}\right) \sin\left(\frac{\phi_{vp}}{2}\right) \cos(J-n)(\theta_{\mathbf{k}} - \theta_{\mathbf{p}}) \\ + \sin\left(\frac{\phi_{ck}}{2}\right) \sin\left(\frac{\phi_{cp}}{2}\right) \cos\left(\frac{\phi_{vk}}{2}\right) \cos\left(\frac{\phi_{vp}}{2}\right) \cos(J-m)(\theta_{\mathbf{k}} - \theta_{\mathbf{p}}) \\ \left. + \sin\left(\frac{\phi_{ck}}{2}\right) \sin\left(\frac{\phi_{cp}}{2}\right) \sin\left(\frac{\phi_{vk}}{2}\right) \sin\left(\frac{\phi_{vp}}{2}\right) \cos(J-m-n)(\theta_{\mathbf{k}} - \theta_{\mathbf{p}}) \right]. \quad (8) \end{aligned}$$

In a simplified model when the interlayer Coulomb interaction $V_{\text{inter}}(k)$ is a constant independent of k , i.e., it is a short-range interaction, one can perform the angle integration, and realize immediately that only when $J = 0, n, m$, and $m + n$, can $|\Delta_{\mathbf{k}}|_J$ be nonzero. As $\phi \in (0, \pi/2)$ and $\cos(\phi/2) > \sin(\phi/2)$, the pairing potential in the $J = 0$ channel is the strongest, and the excitonic pairing is s -wave-like, as shown in Fig. 1(d).

In realistic systems, $V_{\text{inter}}(k)$ is a long-range interaction, and we use the approximate form $V_{\text{inter}}(q) = \frac{2\pi}{\epsilon_r q} e^{-qd}$ hereafter. Here ϵ_r is the dielectric constant of the heterostructure, and d is the distance between the two layers. The mean-field method and the static interlayer interaction adopted in this work are reasonable at least qualitatively, as shown in Refs. [36,37]. We consider two limit cases. First, when D of the GCF model is much larger than αk_F , then ϕ is close to 0, and $\cos(\phi/2) \gg \sin(\phi/2)$. The $J = 0$ channel has the largest pairing strength and the exciton is s -wave-like. Second, in the opposite limit, when $D \rightarrow 0$ and $\cos(\phi/2) \approx \sin(\phi/2) \approx \sqrt{2}/2$, interesting physics occurs. When $m = n$, the pairing in the $J = m$ channel becomes larger than that in the $J = 0$ and $J = 2m$ channels as the second and third terms within the brackets of Eq. (8) merge. The excitonic pairing becomes p -wave-like when $m = 1$ or d -wave-like when $m = 2$, as shown in Figs. 1(e) and 1(f). Assuming that the electron and hole layers are constituted of the same material, we obtain the numerical results of different pairing order parameters using Hartree-Fock equations, and we plot the phase diagram with different D 's and V_g 's for $m = n = 1$ in Fig. 2. We set $\epsilon_r = 5$ and $d = 4$ nm in Figs. 2 and 3 as they are typical experimental conditions, and the picture is robust with different ϵ_r 's and d 's. The excitonic pairing is s -wave-like when D is large, e.g., the TMD systems where $D \approx 1$ eV. For systems with small D , the long-sought high angular momentum exciton condensation may appear, and its material realization is discussed later.

FS projection. The correlation between the angular momentum of the exciton condensation and the band geometry can be seen more clearly when we project the interaction onto the FS. The projection is reasonable in the BCS regime as the pairing order parameter is mainly distributed around the narrow region of the FS [34,38–44], which is also shown in Figs. 1(d)–1(f). Therefore, we can use the

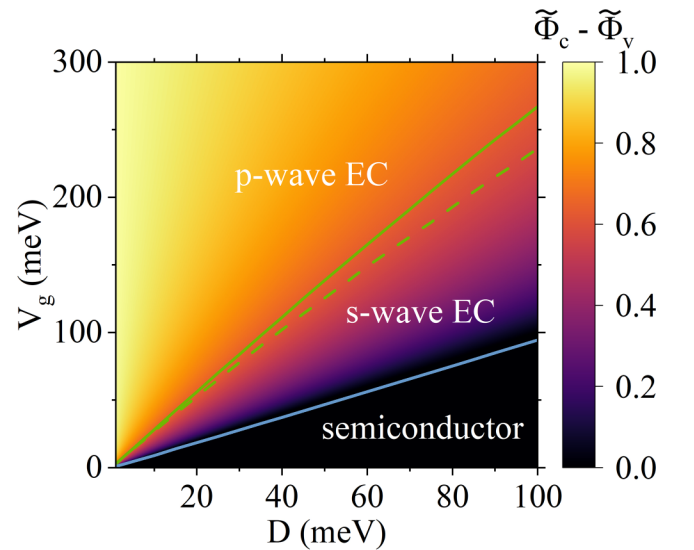


FIG. 2. The phase diagram when the electron and hole layers are both the $m = 1$ GCF model, and $\alpha = 10^6$ m/s. The dielectric constant of the heterostructure is $\epsilon_r = 5$, and the distance between the two layers is $d = 4$ nm. The solid lines are obtained by self-consistent calculations, and the dashed line is determined by the FS projection. The colorbar indicates the Berry curvature flux. EC means exciton condensation.

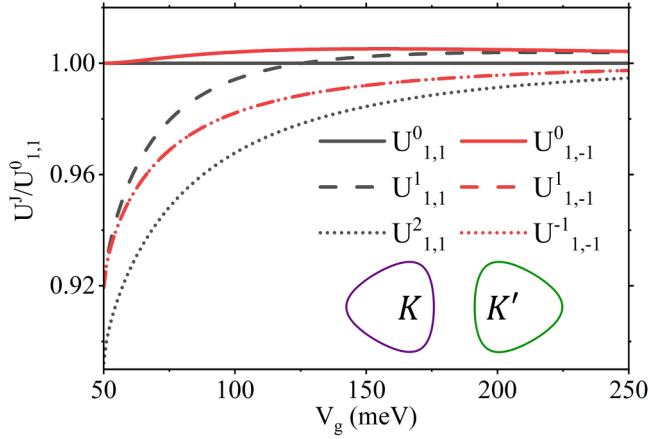


FIG. 3. FS-projected interlayer electron-hole interaction $U^J(k_F)$ for the $|m|=1$ case, where k_F 's vary with different V_g 's. Here $D = 50$ meV, $\varepsilon_r = 5$, and $d = 4$ nm. Inset: FSs for K and K' valleys under a finite trigonal warping effect.

FS-projected interlayer interaction, defined as $U_{m,n}(k_F, \theta_1, \theta_2) \equiv V_{\text{inter}}(k_F, \theta_1, \theta_2) \Lambda_{cc}(k_F, \theta_1, \theta_2) \Lambda_{vv}(k_F, \theta_2, \theta_1)$, to perform an analysis of the angular dependence of the pairing. Decomposing $U_{m,n}$, V_{inter} , Λ_{cc} , and Λ_{vv} into different angular momentum channels and using the convolution rules, we obtain the interaction in each channel J as

$$U_{m,n}^J(k_F) = \sum_{J_1+J_2-J_3=J} V_{\text{inter}}^{J_1}(k_F) \Lambda_{cc}^{J_2}(k_F) \Lambda_{vv}^{J_3}(k_F). \quad (9)$$

The excitonic pairing is characterized by the channel with the largest $U_{\text{inter}}^J(k_F)$. As shown in SM [35], Λ^J 's satisfy the below relations in general rotational symmetric models, as $\sum_J \Lambda^J = 1$ and $\sum_J J \Lambda^J = \frac{\Phi}{2\pi}$, where Φ is the Berry curvature flux through the FS. In this way, the form factors are connected to the band geometry. In the GCF model, only Λ_{cc}^0 , Λ_{vv}^0 , Λ_{cc}^m , and Λ_{vv}^{-n} are nonzero according to Eq. (5). Then the above relations reduce to $\Lambda_{cc}^0 = 1 - \tilde{\Phi}_c/m$, $\Lambda_{vv}^0 = 1 - \tilde{\Phi}_v/n$, $\Lambda_{cc}^m = \tilde{\Phi}_c/m$, and $\Lambda_{vv}^{-n} = \tilde{\Phi}_v/n$, where $\tilde{\Phi} = \Phi/2\pi \in (-|m|/2, |m|/2)$. Taking the long-range form of V_{inter} into consideration, we obtain the s -to- p transition line for $m = n = 1$ in Fig. 2 (dashed green line), which is close to the full numerical calculations. The excitonic pairing is s -wave-like (p -wave-like) when the Berry curvature flux is small (large), which is discussed in detail in the SM [35]. Figure 2 also shows two ways to achieve p -wave EC in experiments, decrease D or increase V_g , which reflects two approaches to increase the Berry flux, increase the Berry flux concentration, or enlarge the FSs. It should be noted that in the trivial case where the form factor is unity, the excitonic pairing always takes place in the $J = 0$ channel, as $V_{\text{inter}}^{J=0}$ is always the largest for the realistic long-range Coulomb interactions. In this way, the GCF model clearly demonstrates the essential role played by band geometry effects in the high angular momentum excitonic pairing.

Material realization. Now we consider how to achieve the p -wave excitonic condensation in realistic materials (the d -wave realization is discussed in the SM [35]). The GCF model can only describe the low-energy physics of real materials. Therefore, we should focus on the small D region,

where the critical V_g will be small correspondingly. In many realistic systems, there are two inequivalent valleys K and K' and two spin indices; therefore, the intervalley and inter-spin pairing channels should be considered in addition. We consider two general time-reversal symmetric Hamiltonians that correspond to many real 2D materials. The first one is $H_1 = v_F(\tau_z \sigma_x k_x - \sigma_y k_y) + \lambda \sigma_z$, where τ_i 's and σ_i 's are Pauli matrices in valley and sublattice spaces, and λ is a real positive number. This is the case of staggered graphene [45–47]. In the presence of time-reversal symmetry, the Berry curvature of the two valleys are opposite, and the chiral winding number is $+1$ (-1) for the K (K') valley. The intra- and intervalley electron-hole interlayer interactions $U_{1,1}^J$ and $U_{1,-1}^J$ in different J channels are shown in Fig. 3, and the intervalley s -wave pairing prevails over the others as $U_{1,-1}^0$ is always the largest. The second one is $H_2 = v_F(\tau_z \sigma_x k_x - \sigma_y k_y) + \lambda \tau_z \sigma_z s_z$, where s_z is the third Pauli matrix in spin space [48] and the last term describes the spin-orbital coupling. This corresponds to the low-energy physics of silicene, germanium [49] and stanene [50]. Now the chiral winding numbers are $1, -1, -1, 1$ for $K \uparrow, K \downarrow, K' \uparrow, K' \downarrow$ species. The interlayer electron-hole interaction for the intraspin intravalley, intraspin intervalley, interspin intravalley, and interspin intervalley channels are $U_{1,1}^J, U_{1,-1}^J, U_{1,-1}^J$, and $U_{1,1}^J$ respectively, and the dominating channels are degenerate intraspin intervalley and interspin intravalley s -wave pairings.

In hexagonal 2D materials, the rotational symmetry of the GCF model is generally degraded down to C_3 by the trigonal warping effect. As shown in the inset of Fig. 3, the perfect nesting between the intervalley FSs will be broken, and the intravalley pairings will prevail over the intervalley pairings. Specifically for the H_1 case, Figure 3 shows that when V_g is large, $U_{1,1}^1$ and $U_{1,-1}^0$ are almost the same, and the intravalley p -wave and intervalley s -wave pairings are nearly degenerate. Now a finite trigonal warping term will make the intravalley p -wave pairing channel the dominant one. Therefore, staggered graphene is a candidate material for the electron and hole layers in Fig. 1(a) to achieve the p -wave exciton condensation [51].

Another way to realize the p -wave exciton condensation is to consider the one-valley systems, i.e., topological surface states, where the top and bottom surface states can be used as the electron and hole layers, respectively, under gating in the heterostructure [Fig. 1(a)]. The surface-state Hamiltonian of a topological insulator thin film reads $H_{\text{tb}} = \pm v_F(k_x s_y - k_y s_x)$ for the top and the bottom surface. When an $M s_z$ term is added to open a gap on both surfaces, the chiral winding numbers for top and bottom layers are both $+1$, and the electron-hole interlayer interaction is $U_{1,1}^J$ in different J channels assuming $M < 0$. According to Fig. 2, the excitonic pairing becomes p -wave when the gating V_g is larger than a moderate critical value, as long as $|M|$ is not too large. This $M s_z$ term can be realized in two systems, i.e., magnetically doped topological insulators and intrinsic axion insulators with higher-order topology [52,53]. The former case can be achieved by doping Cr, V, or Sm in $(\text{Bi}, \text{Sb})_2(\text{Te}, \text{Se})_3$ thin film [54,55]. For the latter case, EuIn_2As_2 can serve as an example, where the surface states have a gap around 10 meV [53]. When the number of the Eu layers is odd, the inversion symmetry is preserved in EuIn_2As_2 , and the top and bottom surface states have a same

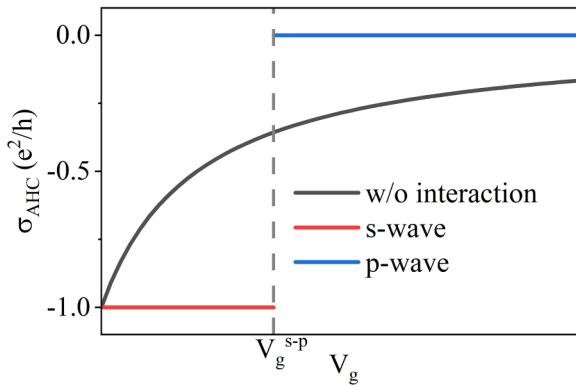


FIG. 4. Anomalous Hall conductivity with (red and blue lines) and without (black solid line) electron-hole interaction in the setup shown in the inset when the gating is increased.

chiral winding number. Therefore, the thin film of magnetically doped topological insulators or intrinsic axion insulators is an achievable setup for p -wave exciton condensation in experiments [56,57].

Experiments. The change in anomalous Hall conductivity can serve as evidence for the p -wave exciton condensation in experiments [58], as shown in Fig. 4. Without the interaction, the Chern numbers of the two valence bands are both $-\frac{1}{2}$ as the chiral winding numbers are both $+1$ in the top and bottom layers. Therefore, the overall anomalous Hall conductivity for this semimetallic system is $\sigma_{\text{AHC}} = \frac{e^2}{h} \int_{\text{occupied}} \frac{d^2k}{(2\pi)^2} \Omega_{n,k} = (\tilde{\Phi}_{c,t} - \tilde{\Phi}_{v,b} - 1) \frac{e^2}{h}$. Including the electron-hole interaction, the system is driven into the insulating excitonic pairing phase. The Chern numbers of the valence bands remain $-\frac{1}{2}$ and $-\frac{1}{2}$ if the pairing is s wave, and they become $\frac{1}{2}$ and $-\frac{1}{2}$ if the pairing is p wave. The anomalous Hall conductivity

of the system becomes $\sigma_{\text{AHC}}^s = [(-\frac{1}{2}) + (-\frac{1}{2})] \frac{e^2}{h} = -\frac{e^2}{h}$ for the s -wave pairing and $\sigma_{\text{AHC}}^p = [(\frac{1}{2}) + (-\frac{1}{2})] \frac{e^2}{h} = 0$ for the p -wave pairing. This can be used as a signature for the exciton condensation not only for the magnetic topological insulator or axion insulator thin film but also for the staggered graphene-based heterostructure, as the electron and hole layers are spin polarized or valley polarized when the gating is not too high [59–62].

In summary, we discussed the high angular momentum exciton condensation induced by band geometric effects. We find that the high angular momentum exciton condensation may appear when the Berry curvature flux through the electron and hole Fermi surfaces is large. This is in analogy to the superconductivity case [63–66], while the attractive interaction is inherent in the exciton case. We also proposed staggered graphene and surface states of magnetically doped topological insulators or intrinsic axion insulators as promising candidates for realizing p -wave exciton condensation and anomalous Hall conductivity as an experimental signature. The high angular momentum exciton condensation may have some exotic properties, such as fractional Josephson effects [67] and exciton anomalous Hall effects [68]. As such, we expect further experimental and theoretical investigations are warranted.

Acknowledgments. We are supported by the National Basic Research Programs of China under Grants No. 2022YFA1403500 and No. 2021YFA1400503; the National Science Foundation of China under Grants No. 12234001, No. 11934003, and No. 62321004; the Beijing Natural Science Foundation under Grant No. Z200004; and the Strategic Priority Research Program of the Chinese Academy of Sciences under Grant No. XDB33010400. The computational resources were provided by the supercomputer center at Peking University, China.

- [1] L. V. Keldysh and Y. V. Kopayev, *Selected Papers of Leonid V Keldysh* (World Scientific, Singapore, 2024), pp. 41–46.
- [2] W. Kohn, *Phys. Rev. Lett.* **19**, 439 (1967).
- [3] D. Jérôme, T. M. Rice, and W. Kohn, *Phys. Rev.* **158**, 462 (1967).
- [4] B. I. Halperin and T. M. Rice, *Rev. Mod. Phys.* **40**, 755 (1968).
- [5] B. Seradjeh, H. Weber, and M. Franz, *Phys. Rev. Lett.* **101**, 246404 (2008).
- [6] B. Seradjeh, J. E. Moore, and M. Franz, *Phys. Rev. Lett.* **103**, 066402 (2009).
- [7] R. Wang, O. Erten, B. Wang, and D. Xing, *Nat. Commun.* **10**, 210 (2019).
- [8] Y. Wu, H. Jiang, H. Chen, H. Liu, J. Liu, and X. C. Xie, *Phys. Rev. Lett.* **128**, 106804 (2022).
- [9] X. Liu, K. Watanabe, T. Taniguchi, B. I. Halperin, and P. Kim, *Nat. Phys.* **13**, 746 (2017).
- [10] J. Li, T. Taniguchi, K. Watanabe, J. Hone, and C. Dean, *Nat. Phys.* **13**, 751 (2017).
- [11] J. Gu, L. Ma, S. Liu, K. Watanabe, T. Taniguchi, J. C. Hone, J. Shan, and K. F. Mak, *Nat. Phys.* **18**, 395 (2022).
- [12] Z. Wang, D. A. Rhodes, K. Watanabe, T. Taniguchi, J. C. Hone, J. Shan, and K. F. Mak, *Nature (London)* **574**, 76 (2019).
- [13] L. Ma, P. X. Nguyen, Z. Wang, Y. Zeng, K. Watanabe, T. Taniguchi, A. H. MacDonald, K. F. Mak, and J. Shan, *Nature (London)* **598**, 585 (2021).
- [14] D. I. Pikulin and T. Hyart, *Phys. Rev. Lett.* **112**, 176403 (2014).
- [15] Q. Zhu, M. W.-Y. Tu, Q. Tong, and W. Yao, *Sci. Adv.* **5**, eaau6120 (2019).
- [16] M. Xie, H. Pan, F. Wu, and S. Das Sarma, *Phys. Rev. Lett.* **131**, 046402 (2023).
- [17] G. Mazza, M. Rösner, L. Windgätter, S. Latini, H. Hübener, A. J. Millis, A. Rubio, and A. Georges, *Phys. Rev. Lett.* **124**, 197601 (2020).
- [18] E. Peretto and G. Stefanucci, *Phys. Rev. Lett.* **125**, 106401 (2020).
- [19] A. Srivastava and A. Imamoğlu, *Phys. Rev. Lett.* **115**, 166802 (2015).
- [20] J. Zhou, W.-Y. Shan, W. Yao, and D. Xiao, *Phys. Rev. Lett.* **115**, 166803 (2015).
- [21] T. Cao, M. Wu, and S. G. Louie, *Phys. Rev. Lett.* **120**, 087402 (2018).
- [22] X. Zhang, W.-Y. Shan, and D. Xiao, *Phys. Rev. Lett.* **120**, 077401 (2018).

- [23] M. M. Glazov, L. E. Golub, G. Wang, X. Marie, T. Amand, and B. Urbaszek, *Phys. Rev. B* **95**, 035311 (2017).
- [24] C. J. Tabert and E. J. Nicol, *Phys. Rev. Lett.* **110**, 197402 (2013).
- [25] D. Xiao, G.-B. Liu, W. Feng, X. Xu, and W. Yao, *Phys. Rev. Lett.* **108**, 196802 (2012).
- [26] H.-Z. Lu, W. Yao, D. Xiao, and S.-Q. Shen, *Phys. Rev. Lett.* **110**, 016806 (2013).
- [27] Y. Gao, S. A. Yang, and Q. Niu, *Phys. Rev. Lett.* **112**, 166601 (2014).
- [28] H. Yu, Y. Wu, G.-B. Liu, X. Xu, and W. Yao, *Phys. Rev. Lett.* **113**, 156603 (2014).
- [29] E. McCann and V. I. Fal'ko, *Phys. Rev. Lett.* **96**, 086805 (2006).
- [30] I. Garate and M. Franz, *Phys. Rev. B* **84**, 045403 (2011).
- [31] H. Yang, J. Zeng, Y. Shao, Y. Xu, X. Dai, and X.-Z. Li, *Phys. Rev. B* **109**, 075167 (2024).
- [32] C. Si, K.-H. Jin, J. Zhou, Z. Sun, and F. Liu, *Nano Lett.* **16**, 6584 (2016).
- [33] Y. Wang, W. Ji, C. Zhang, P. Li, S. Zhang, P. Wang, S. Li, and S. Yan, *Appl. Phys. Lett.* **110**, 213101 (2017).
- [34] J. Zhang and E. Rossi, *Phys. Rev. Lett.* **111**, 086804 (2013).
- [35] See Supplemental Material at <http://link.aps.org/supplemental/10.1103/PhysRevB.109.L201401> for details of the full Hartree-Fock equations, details of the FS projection, and a discussion of possible candidates for *d*-wave exciton condensation, which also includes Ref. [69].
- [36] D. Neilson, A. Perali, and A. R. Hamilton, *Phys. Rev. B* **89**, 060502(R) (2014).
- [37] P. López Ríos, A. Perali, R. J. Needs, and D. Neilson, *Phys. Rev. Lett.* **120**, 177701 (2018).
- [38] X. Zhu, P. B. Littlewood, M. S. Hybertsen, and T. M. Rice, *Phys. Rev. Lett.* **74**, 1633 (1995).
- [39] P. Littlewood, P. Eastham, J. Keeling, F. Marchetti, B. Simons, and M. Szymanska, *J. Phys.: Condens. Matter* **16**, S3597 (2004).
- [40] F. X. Bronold and H. Fehske, *Phys. Rev. B* **74**, 165107 (2006).
- [41] H. Min, R. Bistritzer, J.-J. Su, and A. H. MacDonald, *Phys. Rev. B* **78**, 121401(R) (2008).
- [42] Y.-P. Shim and A. H. MacDonald, *Phys. Rev. B* **79**, 235329 (2009).
- [43] A. Perali, D. Neilson, and A. R. Hamilton, *Phys. Rev. Lett.* **110**, 146803 (2013).
- [44] S. Conti, A. Perali, F. M. Peeters, and D. Neilson, *Phys. Rev. Lett.* **119**, 257002 (2017).
- [45] J. Jung, A. M. DaSilva, A. H. MacDonald, and S. Adam, *Nat. Commun.* **6**, 6308 (2015).
- [46] S. Y. Zhou, G.-H. Gweon, A. Fedorov, P. N. First, W. De Heer, D.-H. Lee, F. Guinea, A. Castro Neto, and A. Lanzara, *Nat. Mater.* **6**, 770 (2007).
- [47] B. Hunt, J. D. Sanchez-Yamagishi, A. F. Young, M. Yankowitz, B. J. LeRoy, K. Watanabe, T. Taniguchi, P. Moon, M. Koshino, P. Jarillo-Herrero *et al.*, *Science* **340**, 1427 (2013).
- [48] C. L. Kane and E. J. Mele, *Phys. Rev. Lett.* **95**, 226801 (2005).
- [49] C.-C. Liu, W. Feng, and Y. Yao, *Phys. Rev. Lett.* **107**, 076802 (2011).
- [50] Y. Xu, B. Yan, H.-J. Zhang, J. Wang, G. Xu, P. Tang, W. Duan, and S.-C. Zhang, *Phys. Rev. Lett.* **111**, 136804 (2013).
- [51] In the SM [35], we show that in gated double-bilayer graphene, *s*-, *p*- and *d*-wave exciton condensation may all appear under different gatings. One previous work [70] has already predicted a phase similar to the *p*-wave exciton condensation in gated double-bilayer graphene, labeled as “BXC” in their work.
- [52] A. M. Essin, J. E. Moore, and D. Vanderbilt, *Phys. Rev. Lett.* **102**, 146805 (2009).
- [53] Y. Xu, Z. Song, Z. Wang, H. Weng, and X. Dai, *Phys. Rev. Lett.* **122**, 256402 (2019).
- [54] M. Mogi, M. Kawamura, A. Tsukazaki, R. Yoshimi, K. S. Takahashi, M. Kawasaki, and Y. Tokura, *Sci. Adv.* **3**, eaao1669 (2017).
- [55] C. Yue, Y. Xu, Z. Song, H. Weng, Y.-M. Lu, C. Fang, and X. Dai, *Nat. Phys.* **15**, 577 (2019).
- [56] C.-Z. Chang, J. Zhang, X. Feng, J. Shen, Z. Zhang, M. Guo, K. Li, Y. Ou, P. Wei, L.-L. Wang *et al.*, *Science* **340**, 167 (2013).
- [57] M. Mogi, Y. Okamura, M. Kawamura, R. Yoshimi, K. Yasuda, A. Tsukazaki, K. Takahashi, T. Morimoto, N. Nagaosa, M. Kawasaki *et al.*, *Nat. Phys.* **18**, 390 (2022).
- [58] N. Nagaosa, J. Sinova, S. Onoda, A. H. MacDonald, and N. P. Ong, *Rev. Mod. Phys.* **82**, 1539 (2010).
- [59] M. Xie and S. Das Sarma, *Phys. Rev. B* **107**, L201119 (2023).
- [60] Y. Jang, Y. Park, J. Jung, and H. Min, *Phys. Rev. B* **108**, L041101 (2023).
- [61] C. Huang, T. M. R. Wolf, W. Qin, N. Wei, I. V. Blinov, and A. H. MacDonald, *Phys. Rev. B* **107**, L121405 (2023).
- [62] Z. Dong, M. Davydova, O. Ogunnaike, and L. Levitov, *Phys. Rev. B* **107**, 075108 (2023).
- [63] J. Shi and Q. Niu, *Sci. China Phys. Mech. Astron.* **63**, 227422 (2020).
- [64] C. Zhang, S. Tewari, R. M. Lutchyn, and S. Das Sarma, *Phys. Rev. Lett.* **101**, 160401 (2008).
- [65] L. Mao, J. Shi, Q. Niu, and C. Zhang, *Phys. Rev. Lett.* **106**, 157003 (2011).
- [66] W. Qin, L. Li, and Z. Zhang, *Nat. Phys.* **15**, 796 (2019).
- [67] H.-J. Kwon, K. Sengupta, and V. M. Yakovenko, *Eur. Phys. J. B* **37**, 349 (2004).
- [68] S. Chaudhary, C. Knapp, and G. Refael, *Phys. Rev. B* **103**, 165119 (2021).
- [69] J. W. F. Venderbos, Y. Hu, and C. L. Kane, *Phys. Rev. B* **98**, 235160 (2018).
- [70] J.-J. Su and A. H. MacDonald, *Phys. Rev. B* **95**, 045416 (2017).